Design of Autonomous and Robust Attitude and Orbit Control System for Very Low Earth Orbit

Pamela Woo Software Developer - Guidance, Navigation and Control, NGC Aerospace Ltd. ROR, Sherbrooke, QC, Canada. pamela.woo@ngcaerospace.com

Marie-Kiki Langelier Software Developer - Guidance, Navigation and Control, NGC Aerospace Ltd. ROR, Sherbrooke, QC, Canada.

Coralie Pelletier-Ouellet Software Developer - Guidance, Navigation and Control, NGC Aerospace Ltd. ROR, Sherbrooke, QC, Canada.

Ludwik A. Sobiesiak Project Manager, NGC Aerospace Ltd. ROR, Sherbrooke, QC, Canada.

Jean-François Hamel Vice-President, Space Systems, NGC Aerospace Ltd. ROR, Sherbrooke, QC, Canada.

ABSTRACT

Very Low Earth Orbit (VLEO) is a region of orbital altitudes below 400 km. Satellite operations in these low altitudes offer many advantages for Earth observation and telecommunications applications. The VLEO region is characterised by strong atmospheric effects, presenting a challenge for Attitude and Orbit Control System (AOCS) design, which must cope with a dominant perturbation that is difficult to model and predict on-board with a high degree of accuracy. This paper presents an autonomous and robust AOCS design suitable for satellite operation in the lower VLEO region, below 200 km. First, a baseline mission concept is defined. Then, novel AOCS functionalities are described, such as the modulation of aerodynamic torques as the primary means of active spacecraft attitude control, and the use of air-breathing electric propulsion for orbit maintenance. Simulation results demonstrate the feasibility of the proposed AOCS design for VLEO operation.

Keywords: Attitude and Orbit Control System, Very Low Earth Orbit

Nomenclature

$\widehat{(\ )}$	=	Denotes an estimated quantity
$(\ )^*$	=	Denotes a commanded or desired quantity
$\widetilde{(\ )}$	=	Denotes an error quantity
$\dot{(\ )}$	=	Denotes first time derivative of a quantity
$(\ )^T$	=	Transpose of a vector or matrix
A_{ref}	=	Spacecraft reference area, a constant parameter
$\vec{B}_x, \vec{B}_y, \vec{B}_z$	=	Spacecraft body x-axis, y-axis, z-axis vectors
$\boldsymbol{C}_M$	=	$[C_l \quad C_m \quad C_n]^T$, Aerodynamic torque coefficients in spacecraft body frame

J = Cost function
L_{ref} = Spacecraft reference length, a constant parameter
$\vec{O}_r, \vec{O}_t, \vec{O}_n$ = Local orbit frame radial, transverse, normal vectors
$\boldsymbol{T}_{aer}$ = Components of the aerodynamic torque vector, expressed in spacecraft body frame
$\vec{r}$ = Spacecraft position vector
$\vec{r}_{sun}$ = Sun position vector
$\vec{v}$ = Spacecraft velocity vector
v_{rel} = Spacecraft air-relative velocity magnitude
$\vec{v}_{rel}$ = Spacecraft air-relative velocity vector
$\vec{v}_{wind}$ = Wind velocity vector
$\boldsymbol{\Gamma}$ = Adaptation law gain matrix
α = Angle of attack
β = Angle of sideslip
$\boldsymbol{\delta}$ = $[\delta_1 \quad \delta_2 \quad \delta_3 \quad \delta_4]^T$, Solar array panel deflections
ρ_{atm} = Atmospheric density
$\boldsymbol{\chi}$ = Vector of parameters
$\vec{\omega}_{\oplus}$ = Earth angular velocity vector
$\tilde{\boldsymbol{\omega}}$ = A function of attitude and angular velocity control errors

Bolded variables refer to column vector or matrix quantities.

1 Introduction

Very Low Earth Orbit (VLEO) is a region of orbital altitudes below 400 km. Satellite operation in these low altitudes offers many benefits, such as enhanced resolution for Earth observation applications, and greater signal strength and lower latency for telecommunications applications [1]. On the other hand, the VLEO region is characterised by stronger atmospheric effects, presenting a challenge for Attitude and Orbit Control System (AOCS) design, which must cope with a dominant aerodynamic perturbation that is difficult to model and predict on-board with a high degree of accuracy.

Current VLEO mission designs target operational altitudes at the upper VLEO regime, between 250 km and 300 km. These altitudes are appealing to spacecraft platform providers since the attitude and orbit control requirements can be achieved using conventional flight-proven AOCS sensors and actuators, yielding a relatively quick path to market for the concept platform.

However, conventional AOCS equipment are not suitable when operating in the lower VLEO regime, for altitudes lower than 250 km. Namely, due to the increase in atmospheric drag leading to faster rate of altitude decay, more frequent orbit maintenance manoeuvres are required, increasing the propellant mass budget. Rejection of the aerodynamic torque disturbances leads to faster saturation of reaction wheels, requiring either increased wheel capacity or large magnetic torque rods to facilitate frequent momentum dumping; either option incurs an undesirable mass penalty.

Alternatively, the AOCS can use unconventional actuators that can leverage the increased aerodynamic effects found in the VLEO environment: articulated appendages can be used to modulate the aerodynamic torque for attitude control, and air-breathing propulsion can exploit the increased atmospheric density to generate thrust for orbit control without the need for on-board propellant.

The goal of this study is to design an autonomous and robust AOCS suitable for satellite operation in the lower VLEO region, below 200 km, where operation of air-breathing electric propulsion is viable. First, a mission concept is defined. Then, novel AOCS functionalities are described, such as the modulation of aerodynamic torques as the primary means of active spacecraft attitude control, and the use of air-breathing electric propulsion for orbit maintenance. Finally, the feasibility of the proposed AOCS design for VLEO is demonstrated by simulation in MATLAB/Simulink.

2 VLEO Mission Concept

The mission concept (derived from the one presented in [3]) is a constellation of satellites, in near-circular orbit at altitudes between 170 km and 190 km, using multiple orbit planes at 75 deg inclination, to provide global coverage of a significant number of northern communities for telecommunications.

3 AOCS Hardware

The concept spacecraft is illustrated in Fig. 1. The spacecraft consists of a central spacecraft bus with two pairs of solar arrays oriented orthogonal to each other. In nominal flight, the spacecraft +x-axis is roughly along the velocity direction for minimal drag, and the payload direction (spacecraft +z-axis) is roughly towards nadir. Since the orbit can have any Local Time of Ascending Node (LTAN), there must be a sufficient number of solar panels exposed to the Sun at any time. Thus, all four arrays are plated on both sides with solar panels. To maximise solar panel illumination, roll-steering can be performed while continuing to maintain a minimal drag orientation.

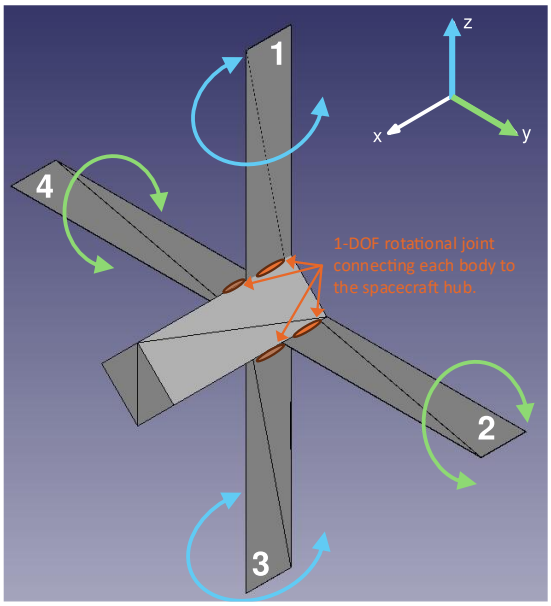

Fig. 1 Spacecraft with Four Articular Solar Array Panels

Additionally, each solar array is capable of rotation about its respective longitudinal axis (arrays 1 and 3 about the body z-axis, arrays 2 and 4 about the body y-axis). By rotating the solar arrays with respect to the incoming atmospheric flow, a desired aerodynamic torque can be generated for the purpose of attitude control, in similar fashion to how aircraft control surfaces change the aerodynamic torque acting on an aircraft.

Aerodynamic control is most effective when the spacecraft longitudinal axis is coarsely aligned with the direction of flight. Magnetic torque rods are required to perform the initial detumbling of the spacecraft. A single reaction wheel oriented along the −y-axis is also baselined. When commanded at fixed speed, the reaction wheel generates a momentum bias that coarsely aligns the spacecraft −y-axis with the orbit normal. Magnetic torque rods are used to roughly align the x-axis along the flight direction before active aerodynamic control can be initiated.

The concept spacecraft is equipped with an Air-Breathing Electric Thruster (ABET) for orbit control. It is a type of thruster that uses electrical energy to ionise and accelerate incoming atmospheric molecules to generate thrust, rather than using an on-board propellant such as Xenon or Kypton [2]. Thus, the spacecraft is effectively supplied with renewable propellant, extending its lifetime considerably. With electric propulsion, very high exhaust velocities are possible, resulting in correspondingly high specific

impulses, but the magnitude of the generated thrust is much smaller than with conventional chemical propulsion. Their high specific impulse permits electric thrusters to realise propulsive manoeuvres with significantly less propellant than chemical thrusters, but over a longer duration of time. The high-efficiency/low-thrust nature of electric propulsion is ideal for compensation of the persistent low-magnitude atmospheric drag found in the VLEO environment. However, there is a lower threshold in atmospheric density for use of the ABET, rendering their operation only viable in the lower VLEO range, between 160 km and 195 km in altitude, the range in which the drag force can still be overcome by the low thrust generated by the ABET. The ABET intake must be along the incoming flow, so the thrust direction is constrained roughly along the velocity vector. This constraint imposes limitations on both the orbit and attitude manoeuvres that can be performed by the spacecraft.

For navigation, the spacecraft is equipped with a suite of conventional sensors: a GNSS receiver for orbit determination and three star trackers for attitude determination.

4 Novel AOCS Software Functions for VLEO

The AOCS software provides the following top-level functions:

- Navigation: Consists of the determination of the current dynamical state (orbit, attitude) of the spacecraft from measurements.
- Guidance: Consists of the computation of the desired or commanded dynamical state of the spacecraft.
- Control: Consists of the determination and execution of the necessary control commands that will bring the current dynamical state of the spacecraft coincident with the desired state.

A simplified functional architecture of the AOCS software, showing the core functions, is shown in Fig. 2. Highlighted in **blue bold** text are novel AOCS functions developed for spacecraft operating in VLEO. These functions are described next.

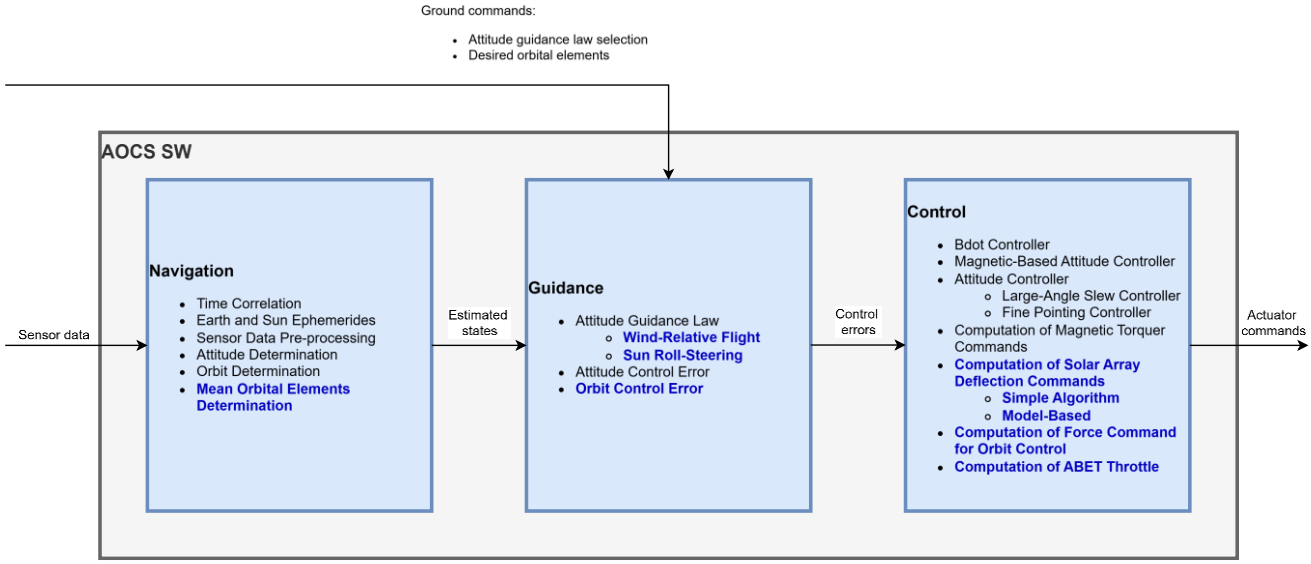

Fig. 2 Simplified Functional Architecture of the AOCS Software

4.1 Air-Relative Attitude Guidance

In general, the attitude guidance law computes the desired spacecraft attitude, angular velocity, and angular acceleration profile to align the spacecraft with a desired reference frame. For spacecraft operating in VLEO, two guidance modes are considered:

- Wind-Relative Flight mode
- Sun Roll-Steering mode

4.1.1 Wind-Relative Flight Mode Guidance

For minimal drag, the Wind-Relative Flight mode guidance law is developed, to align the spacecraft longitudinal axis (+x-axis) with the air-relative velocity:

$$\vec{B}_x^* = \frac{\hat{\vec{v}}_{rel}}{\left|\hat{\vec{v}}_{rel}\right|} \tag{1}$$

The complete form of the air-relative velocity is given by Section 8.6.2 of [4]:

$$\vec{v}_{rel} = \vec{v} - \vec{\omega}_{\oplus} \times \vec{r} - \vec{v}_{wind} \tag{2}$$

On-board knowledge of the wind velocity is not available, so the last term of (2) is neglected and the atmosphere is assumed to be rotating with the Earth:

$$\hat{\vec{v}}_{rel} = \hat{\vec{v}} - \hat{\vec{\omega}}_{\oplus} \times \hat{\vec{r}} \tag{3}$$

Additionally, the Wind-Relative Flight mode guidance law points the payload direction (+z-axis) roughly towards nadir, with:

$$\vec{B}_z^* = \frac{\hat{\vec{O}}_n \times \vec{B}_x^*}{\left|\hat{\vec{O}}_n \times \vec{B}_x^*\right|} \tag{4}$$

The spacecraft position and velocity, Earth angular velocity, and orbit normal direction are quantities estimated by the Navigation function.

4.1.2 Sun Roll-Steering Mode Guidance

For minimal drag, the Sun Roll-Steering frame guidance law is developed, to align the spacecraft longitudinal axis (+x-axis) with the air-relative velocity, as given in Eq. (1). Additionally, the guidance law rotates the spacecraft around the roll axis to maximise solar panel illumination, by minimising the Sun incidence angle with the solar arrays, with:

$$\vec{B}_z^* = \frac{\hat{\vec{r}}_{sun} \times \vec{B}_x^*}{\left|\hat{\vec{r}}_{sun} \times \vec{B}_x^*\right|} \tag{5}$$

Depending on the LTAN of the orbit, Eq. (5) results in either $\vec{B}_z^*$ pointing towards the Earth (desired) or away from the Earth (undesired). Therefore, Eq. (5) is modified to ensure $\vec{B}_z^*$ points towards nadir:

$$\vec{B}_z^* = \text{sign}\left(\left(\hat{\vec{r}}_{sun} \times \vec{B}_x^*\right) \cdot \left(-\hat{\vec{O}}_r\right)\right) \frac{\hat{\vec{r}}_{sun} \times \vec{B}_x^*}{\left|\hat{\vec{r}}_{sun} \times \vec{B}_x^*\right|} \tag{6}$$

The Sun direction and orbit radial direction are quantities estimated by the Navigation function.

4.2 Computation of Solar Array Deflection Commands for Aerodynamic Attitude Control

The aerodynamic torque acting on the spacecraft is a function of two fundamental things: the dynamic pressure of the flow and the geometry of the spacecraft relative to the incoming flow. The dynamic pressure is a function of the spacecraft velocity relative to the atmosphere and the local atmospheric density. Both velocity and density are functions of orbit altitude, and other environmental variables (such as level of solar activity). The spacecraft geometry can be manipulated to modulate the aerodynamic torque. The aerodynamic torque acting on the spacecraft can be modelled as:

$$\boldsymbol{T}_{aer} = \frac{1}{2}\rho_{atm} v_{rel}^2 A_{ref} L_{ref} \boldsymbol{C}_M \tag{7}$$

where the aerodynamic torque coefficients $\boldsymbol{C}_M$ are functions of the spacecraft angle of attack, angle of sideslip, and panel deflections:

$$\boldsymbol{C}_M \equiv \begin{bmatrix} C_l(\alpha, \beta, \boldsymbol{\delta}) \\ C_m(\alpha, \beta, \boldsymbol{\delta}) \\ C_n(\alpha, \beta, \boldsymbol{\delta}) \end{bmatrix} \tag{8}$$

For a given desired aerodynamic control torque $\boldsymbol{T}_{aer}^*$, Eq. (7) is re-arranged to:

$$\boldsymbol{C}_M^* = \begin{bmatrix} C_l(\alpha, \beta, \boldsymbol{\delta}^*) \\ C_m(\alpha, \beta, \boldsymbol{\delta}^*) \\ C_n(\alpha, \beta, \boldsymbol{\delta}^*) \end{bmatrix} = \frac{\boldsymbol{T}_{aer}^*}{\frac{1}{2}\hat{\rho}_{atm} \hat{v}_{rel}^2 A_{ref} L_{ref}} \tag{9}$$

The control torque allocation problem consists of determining the panel deflections $\boldsymbol{\delta}^*$ required to produce the desired aerodynamic coefficient $\boldsymbol{C}_M^*$ for attitude control. The determination of $\boldsymbol{\delta}^*$ to realise the desired control torque is the main challenge of the panel allocation problem, as the desired aerodynamic torque coefficients $\boldsymbol{C}_M^*$ are nonlinear functions of the desired panel deflections so there is no analytical solution for $\boldsymbol{\delta}^*$.

For the baseline AOCS design, two algorithms are retained:

1. Model-based online minimisation of the command error;
2. Fundamental control action strategy, with decoupled (per-axis) linear approximation and fixed timing cycle.

4.2.1 Model-Based Minimisation of the Command Error

The estimated aerodynamic torque coefficients are expressed as closed-form functions of the panel deflections, based on the Sentman drag plate model, presented in Section III.A of [5]:

$$\widehat{\boldsymbol{C}}_M(\boldsymbol{\delta}^*) = \begin{bmatrix} C_l(\hat{\alpha}, \hat{\beta}, \boldsymbol{\delta}^*) \\ C_m(\hat{\alpha}, \hat{\beta}, \boldsymbol{\delta}^*) \\ C_n(\hat{\alpha}, \hat{\beta}, \boldsymbol{\delta}^*) \end{bmatrix} \tag{10}$$

The estimated angle of attack and angle of sideslip are obtained from the Navigation function. The command error is defined:

$$\widetilde{\boldsymbol{C}}_{\boldsymbol{M}} = \boldsymbol{C}_M^* - \widehat{\boldsymbol{C}}_M(\boldsymbol{\delta}^*) \tag{11}$$

where $\boldsymbol{C}_M^*$ is the desired aerodynamic torque coefficients to produce the aerodynamic torque, obtained from Eq. (9). The local dynamic pressure $\frac{1}{2}\hat{\rho}_{atm}\hat{v}_{rel}^2$ is computed from the estimated spacecraft orbital states obtained from the Navigation function.

The function uses an optimisation algorithm to compute the panel deflection commands $\boldsymbol{\delta}^*$ that minimise the cost function $J = \frac{1}{2}\widetilde{\boldsymbol{C}}_{\boldsymbol{M}}{}^T\widetilde{\boldsymbol{C}}_{\boldsymbol{M}}$, using the iterative Gauss-Newton update:

$$\Delta\boldsymbol{\delta}_k = \left(\frac{\partial\widehat{\boldsymbol{C}}_M}{\partial\boldsymbol{\delta}}^T\frac{\partial\widehat{\boldsymbol{C}}_M}{\partial\boldsymbol{\delta}}\right)^{-1}\left(\frac{\partial\widehat{\boldsymbol{C}}_M}{\partial\boldsymbol{\delta}}\right)^T\widetilde{\boldsymbol{C}}_{\boldsymbol{M}}(\boldsymbol{\delta}_k) \tag{12}$$

where the index k denotes the current iteration. The panel deflection command update at the current iteration is then:

$$\boldsymbol{\delta}_{k+1} = \boldsymbol{\delta}_k + \Delta\boldsymbol{\delta}_k \tag{13}$$

The solution for $\boldsymbol{\delta}^*$ is obtained by performing iterations of Eq. (12) and Eq. (13), stopping when J is below a tolerance, or a maximum number of iterations is reached. Although in testing it was observed that the function always converged to a panel deflection solution, convergence to a solution is not necessarily guaranteed.

4.2.2 Fundamental Control Action Strategy

A simpler, alternative panel allocation strategy was designed as a fallback algorithm in the event the model-based optimisation algorithm could not find a solution. This algorithm is simple when compared to the model-based optimisation approach and has no convergence issues but is limited in its ability to yield a deflection solution that will produce the desired three-dimensional control torque.

For the spacecraft concept of Fig. 1, assuming the spacecraft longitudinal axis is coarsely aligned with the air-relative velocity (aided by the spacecraft's passive aero-stability), the set of equations in Eq. (8) can be reduced to a set of decoupled aerodynamic torque coefficients around each body axis, if the panel deflections are limited to the following fundamental control actions:

- Aileron action: Equal and opposite deflections of panels 1 and 3, and panels 2 and 4, to produce a roll torque (about x-axis),
- Elevator action: Equal deflections of panels 2 and 4 to produce a pitch torque (about y-axis),
- Rudder action: Equal deflections of panels 1 and 3 to produce a yaw torque (about z-axis).

The resulting torques produced by the fundamental control actions are:

$$\begin{aligned}\boldsymbol{T}_x &= [C_{l,simple}(\boldsymbol{\delta}_{ail}) \quad 0 \quad 0]^T\\ \boldsymbol{T}_y &= [0 \quad C_{m,simple}(\boldsymbol{\delta}_{ele}) \quad 0]^T\\ \boldsymbol{T}_z &= [0 \quad 0 \quad C_{n,simple}(\boldsymbol{\delta}_{rud})]^T\end{aligned} \tag{14}$$

where the fundamental control actions are:

$$\begin{aligned}\boldsymbol{\delta}_{ail} &= [\delta_{ail} \quad \delta_{ail} \quad -\delta_{ail} \quad -\delta_{ail}]^T\\ \boldsymbol{\delta}_{ele} &= [0 \quad \delta_{ele} \quad 0 \quad \delta_{ele}]^T\\ \boldsymbol{\delta}_{rud} &= [\delta_{rud} \quad 0 \quad \delta_{rud} \quad 0]^T\end{aligned} \tag{15}$$

and δ_{ail}, δ_{ele}, δ_{rud} are the computed panel deflections to achieve the desired control torque.

For a small panel deflections angles around the zero, the torque generated by a fundamental control action scales linearly with the deflection angle, making it straightforward to compute a panel deflection

given a desired torque. Unfortunately, the linear combination of these fundamental actions does not result in a linear combination of the resulting aerodynamic torques. One approach to circumvent this complication is to limit allocation to only one of the fundamental control actions at a time.

The fundamental control action strategy consists of holding the desired aerodynamic control torque for a given control period and sequentially commanding one fundamental control action at a time to realise a single component of the control over a given sub-period of the total control period. The control period is divided into three equal sub-periods, one per body-axis component of the control torque. The selection of the total control period is not straightforward: it must be long enough so that the different torque components are realised for a meaningful amount of time, but short enough that one axis is not left uncontrolled for too long. It must also be sufficiently long enough to respect the bandwidth of the panel drive mechanism. For the baseline design, a total control period of 33 s is selected (11 s per body axis).

The fundamental control action strategy does not produce the desired control torque instantaneously, but rather realises the control torque in an averaged sense over the control period. However, there are no questions of convergence using this strategy, as the simple torque-to-deflection mapping will always yield a solution. The strategy is therefore retained in the AOCS design as a redundant algorithm. The selection between the two algorithms is up to the AOCS User (e.g., Ground operator).

4.3 Orbit Control

An on-board orbit control loop is developed to compute, in real-time, the desired force and ABET command for orbit maintenance. For greater autonomy, the only Ground inputs are the desired orbital elements to be maintained: the reference semi-major axis, eccentricity, and inclination. The computation of propulsive manoeuvres is performed entirely on-board.

The Navigation function relies on the spacecraft's GNSS sensor to estimate accurate orbital states. However, these are osculating orbital elements that exhibit short- and long-period oscillations due to the various perturbations experienced by the spacecraft. The short-term oscillations in particular are undesirable in an orbit maintenance feedback control law since their presence can result in unnecessary controller actuation.

Mean orbital elements provide a way to model the secular change of orbital elements due to one or several perturbations while removing the periodic oscillations. Using the mean orbital elements, an orbit control law is developed, based on Section 14.8 of [6], to compute the control force required to compensate for the secular changes. Whenever the control force is greater than a minimum threshold, i.e., the orbit control error is sufficiently large, the control force is mapped to a thruster throttle command, automatically initiating a propulsive manoeuvre.

5 AOCS Design Validation

A complete and integrated AOCS software is currently under validation, using NGC's in-house high-fidelity simulator in MATLAB/Simulink, which includes models of:

- Spacecraft attitude and orbital dynamics;
- VLEO environment: atmospheric density, wind speed, magnetic field, gravity field;
- Perturbation torques and forces: aerodynamic drag, magnetic perturbation, gravitational perturbation from nonspherical Earth, gravity gradient, solar radiation pressure;
- Earth, Sun, Moon ephemerides;

- Sensors;
- Actuators.

This paper presents the results of the following test cases:

1. Transition from detumbling to wind-relative flight
2. Sun roll-steering functionalities
3. Sun roll-steering performance

The first two test cases are single simulations that verify AOCS functionality. As such, only phenomena taken into account by the AOCS software are modelled, e.g., sensors and actuators characteristics. The third test case is a Monte Carlo simulation—which includes other phenomena such as star tracker misalignments, spacecraft centre of mass and inertia knowledge errors, variations in initial conditions, etc.—used to evaluate the AOCS performance.

The simulation conditions are summarised in Table 1.

Table 1 Simulation conditions for AOCS design validation

	Test Cases 1 and 2	Test Case 3
Simulation Type	Single	Monte Carlo (200 simulations)
Atmosphere Model F10.7 index	140	Random value 25-300
Atmosphere Model Ap index	15	Random value 1-240
Spacecraft Mass	300 kg	
Spacecraft Principal Inertias	[92.2, 123.2, 123.2] kg.m^2	
Spacecraft Centre of Mass Knowledge Error	0	Up to +/-50 mm per axis
Spacecraft Inertia Knowledge Error	0	Up to +/-20% per inertia element
GNSS Position Error	5 m per axis in terrestrial frame	
GNSS Velocity Error	0.1 m/s per axis in terrestrial frame	
Star Tracker Noise	4.5 arcsec (3σ) across boresight 30 arcsec (3σ) around boresight	
Star Tracker Alignment Knowledge Error	0	Up to 30 arcsec total per star tracker unit
Solar Array Drive Mechanism (SADM) Output Step Size	0.0375 deg	
SADM Maximum Rate	1 deg/s	
ABET Maximum Thrust	25 mN	
Initial Date	Spring 2025	Random day Spring 2025 and Spring 2026
Initial Orbit Altitude	180 km	Random value 170-190 km
Initial Orbit Eccentricity	0	Random value 0-0.001

Initial Orbit Right Ascension of the Ascending Node	90 deg	Random value 0-360 deg
Initial Orbit Inclination	75 deg	
Initial True Anomaly	0 deg	Random value 0-360 deg
Initial Attitude	20 deg offset from local orbital frame	Up to 20 deg offset from local orbital frame, in any direction
Initial Angular Velocity	0.05 deg/s per body axis	Up to +/-0.05 deg/s per body axis, in any direction

5.1 Wind-Relative Flight

The objective of this test is to verify that magnetic actuation can detumble the spacecraft from launcher separation conditions, and coarsely align the spacecraft with the incoming flow, to allow transition to Wind-Relative Flight mode.

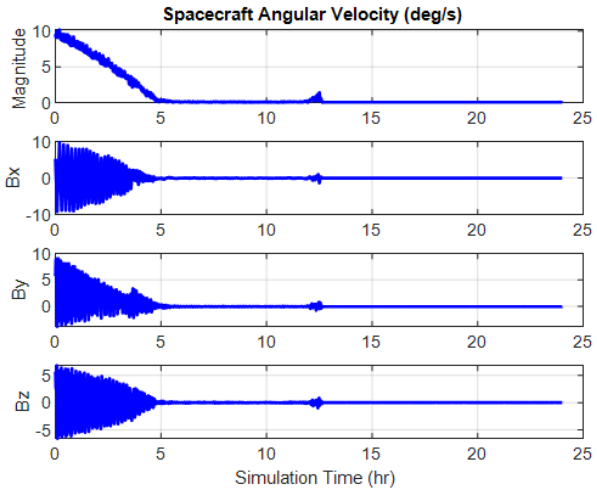

Fig. 3 Wind-Relative Flight – Spacecraft Angular Velocity

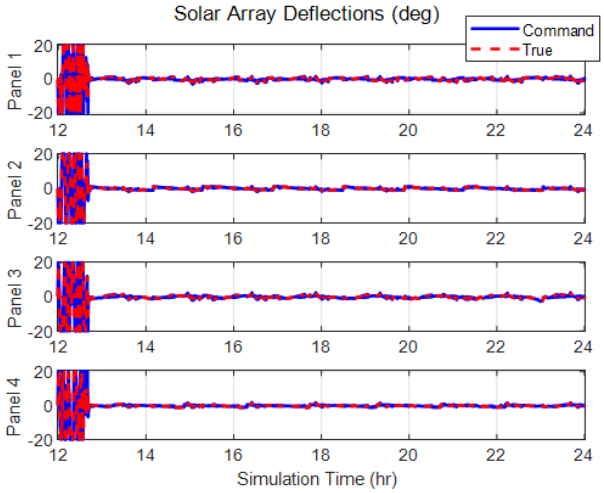

Fig. 4 Wind-Relative Flight – Solar Array Panel Deflections

In this test, the spacecraft starts at the worst-case tip-off rate of 6 deg/s per axis. For the first 12 hours, magnetic actuation is used to detumble the spacecraft, to less than 0.2 deg/s, as shown in Fig. 3.

After 12 hours, the spacecraft enters Wind-Relative Flight mode. Magnetic actuation stops, and aerodynamic control is initiated, as shown by the solar array panels deflections in Fig. 4. For around one hour, the panel deflections are driven to the maximum allowable rotations of ± 20 deg, to reduce the residual angular rate. After this initial convergence time, the panel deflections remain close to the minimal drag configuration of zero deflection. Fig. 5 shows the spacecraft x-axis is controlled to within 1.5 deg of the air-relative velocity, and the z-axis is within 0.2 deg of nadir, demonstrating that aerodynamic control alone is capable of maintaining the spacecraft attitude.

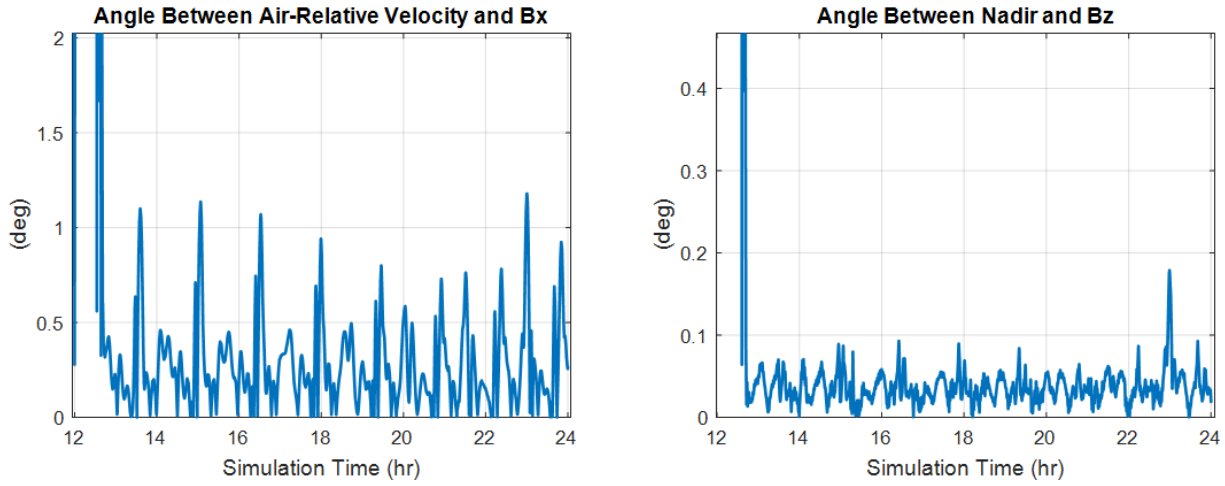

Fig. 5 Wind-Relative Flight – Spacecraft Pointing

In this test, orbit control is enabled only during Wind-Relative Flight mode, starting at 12 hours. Fig. 6 shows that the initial orbit has decayed by 20 km during the initial detumbling. Once orbit control is enabled, the ABET is commanded and constantly operated at full throttle, and the orbit mean semi-major axis is maintained at around 6540 km. It is noted that at this altitude of around 162 km, the ABET provides sufficient thrust to maintain the altitude, but is unable to raise the orbit to the Ground-commanded mean semi-major axis of 6558 km. This test demonstrates a limit on the altitude at which the ABET is capable of compensating for orbit decay. It is noted that this lower altitude threshold varies with environmental conditions (such as the level of solar activity). In this test, moderate solar activity is simulated.

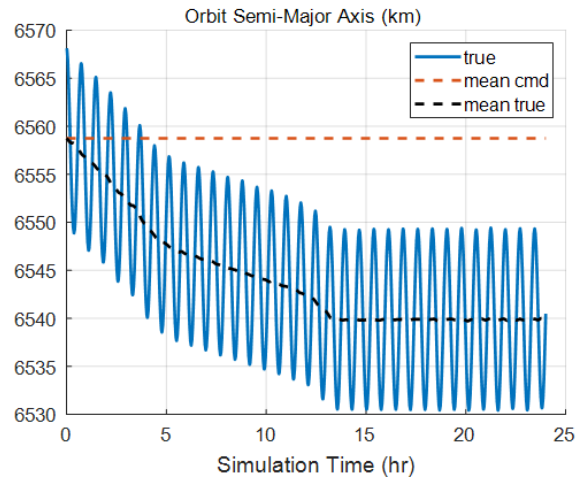

Fig. 6 Wind-Relative Flight – Orbit Semi-Major Axis

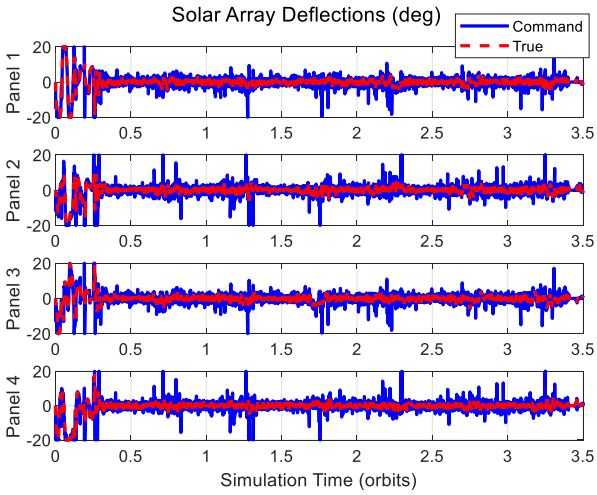

Fig. 7 Sun Roll-Steering – Solar Array Panel Deflections

5.2 Sun Roll-Steering Functionalities

The objective of this test is to verify the AOCS functionalities in Sun Roll-Steering mode. The simulation starts with the spacecraft already coarsely aligned with the air-relative velocity.

The model-based panel allocation function is used to compute the solar array deflections. Fig. 7 shows panel deflection commands and the tracking of those commands by the true panels. A maximum panel rotation speed of 1 deg/s limits perfect tracking of the command. Despite this limitation, the spacecraft attitude tracks the desired attitude, achieving sub-1000 arcsec pointing error, once converged (see Fig 8.).

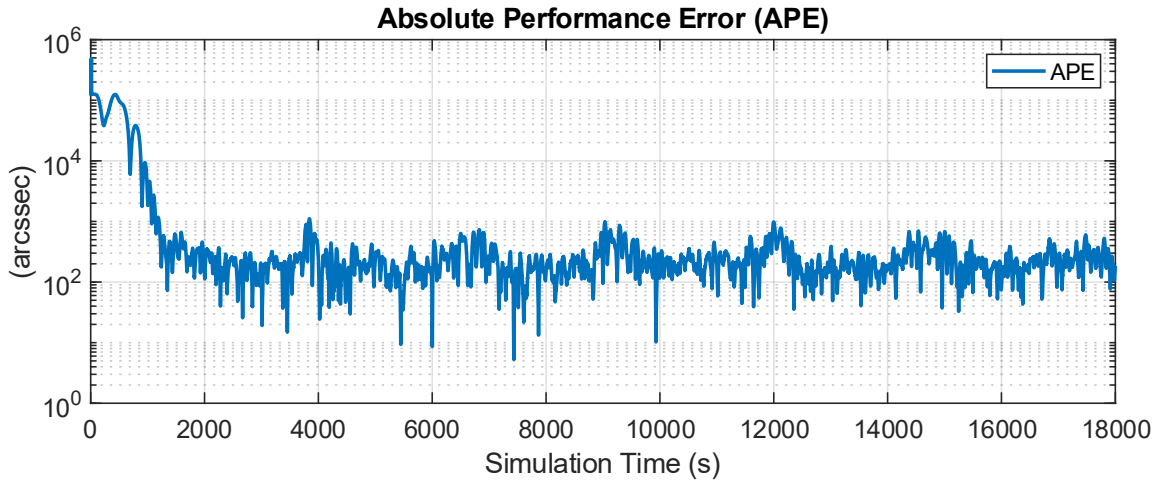

Fig. 8 Sun Roll-Steering – Pointing Error

Fig. 9 shows the spacecraft x-axis is controlled to within 2 deg of the air-relative velocity. As the spacecraft is constrained to roll-steering only (by the guidance law), perfect Sun-pointing of the solar array normal is not possible. As seen in Fig. 9, the angle between the Sun direction and the solar array along −y-axis oscillates up to around 12 deg for the simulated orbit, twice per orbit. This test demonstrates the functionality of the AOCS to provide Sun roll-steering using only aerodynamic control torque.

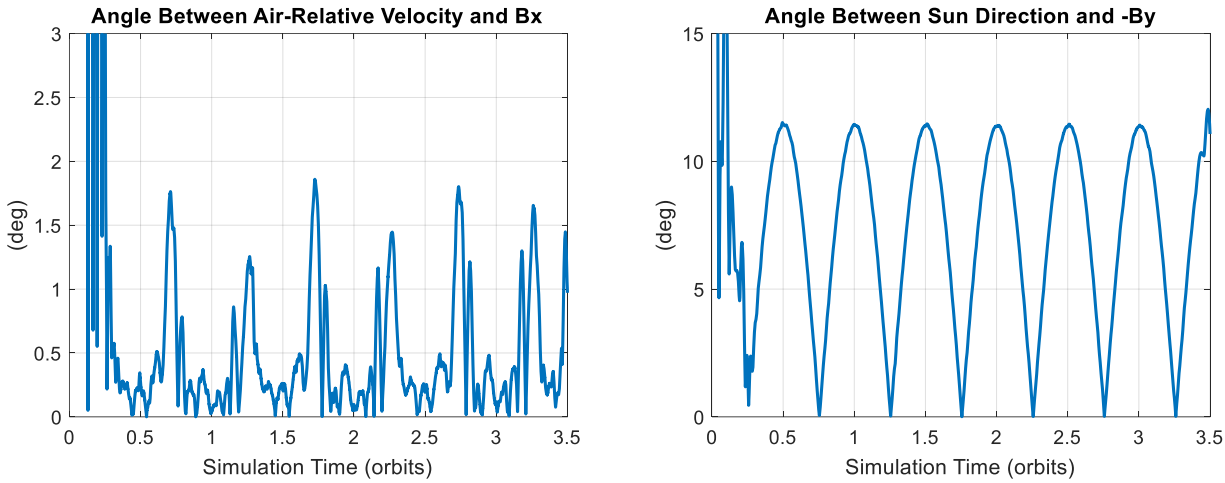

Fig. 9 Sun Roll-Steering – Spacecraft Pointing

5.3 Sun Roll-Steering Performance

The objective of this test is to verify the AOCS performance in Sun Roll-Steering mode.

When using the model-based approach for control torque allocation, the achieved pointing performance is an Absolute Performance Error (APE) of less than 1.35 deg (95% confidence).

The orbit control performance achieved is:

- Mean semi-major axis error: less than 190 m
- Mean eccentricity error: less than 1.24e-4

6 Conclusions

This paper presented an autonomous and robust AOCS design suitable for satellite operation in the lower VLEO region, below 200 km, where atmospheric effects are dominant. Instead of conventional actuators such as reaction wheels, the spacecraft geometry is manipulated via rotations of the solar arrays,

exploiting the aerodynamic torque for attitude control. For orbit control, an ABET generates the thrust needed to correct for altitude decay, by using the surrounding air molecules, an effectively infinite resource. Simulations in MATLAB/Simulink demonstrate the feasibility of the proposed AOCS design. Through a Monte Carlo testing campaign, the AOCS achieves pointing performance in the order of 1.35 deg in APE when using the proposed model-based approach for control torque allocation to compute solar array deflection commands for aerodynamic attitude control.

Acknowledgments

The authors acknowledge the financial support of the European Space Agency (ESA).

Declaration of Use of Artificial Intelligence

Artificial intelligence was not used in the work presented.

References

[1] Chan Yuk Chi, Indraji Ushantha Wanigaratne, and David Dubinsky. How low can you go: Advocating Very Low Earth Orbit as the next frontier for satellite operations. In *Proceedings of the 8th European Conference on Space Debris (virtual)*, Darmstadt, Germany, 20–23 April 2021.

[2] Tommaso Andreussi, Eugenio Ferrato, and Vittorio Giannetti. A review of air-breathing electric propulsion: from mission studies to technology verification. *Journal of Electric Propulsion*, 1, December 2022. doi: 10.1007/s44205-022-00024-9.

[3] Lucy Berthoud, Russell Hills, Andrew Bacon, Michael Havouzaris-Waller, Kieran Hayward, Jean-Didier Gayrard, Fabrice Arnal, and Laurent Combelles. Are Very Low Earth Orbit (VLEO) satellites a solution for tomorrow's telecommunication needs? *CEAS Space Journal*, 14(4), June 2022. doi: 10.1007/s12567-022-00437-0.

[4] David A. Vallado. *Fundamentals of Astrodynamics and Applications, Fourth Edition*. Microcosm Press, 2013.

[5] Lee H. Sentman, L. H. Free Molecule Flow Theory and Its Application to the Determination of Aerodynamic Forces. Lockheed Missiles & Space Company, Technical Report LMSC-448514, 1961.

[6] Hanspeter Schaub John L. Junkins, "Relative Orbit Control Methods," *Analytic Mechanics of Space Systems, Second Edition*, AIAA, Reston ,VA, 2009, pp. 729–747